

R-matrix calculations for opacities: III. Plasma broadening of autoionizing resonances

A K Pradhan^{1,2,3} 

¹ Department of Astronomy, Ohio State University, Columbus, OH 43210, United States of America

² Chemical Physics Program, Ohio State University, Columbus, OH 43210, United States of America

³ Biophysics Graduate Program, Ohio State University, Columbus, OH 43210, United States of America

E-mail: pradhan.1@osu.edu

Received 23 August 2023, revised 28 February 2024

Accepted for publication 23 April 2024

Published 17 May 2024



Abstract

A general formulation is employed to study and quantitatively ascertain the effect of plasma broadening of *intrinsic* autoionizing (AI) resonances in photoionization cross sections. In particular, R-matrix data for iron ions described in the previous paper in the RMOP series (RMOP-II, hereafter RMOP2) are used to demonstrate underlying physical mechanisms due to electron collisions, ion microfields (Stark), thermal Doppler effects, core excitations, and free–free transitions. Breit–Pauli R-matrix cross sections for a large number of bound levels of Fe ions are considered, 454 levels of Fe XVII, 1184 levels of Fe XVIII and 508 levels of Fe XIX. Following a description of theoretical and computational methods, a sample of results is presented to show significant broadening and shifting of AI resonances due to *extrinsic* plasma broadening as a function of temperature and density. The redistribution of AI resonance strengths broadly preserves their integrated strengths as well as the naturally *intrinsic* asymmetric shapes of resonance complexes which are broadened, smeared and flattened, eventually dissolving into the bound-free continua.

Keywords: autoionizing resonances, plasma broadening effects, astrophysics and plasma physics

1. Introduction

Resonances arise in most atomic interactions. They are especially important in processes such as ($e + \text{ion}$) scattering and photoionization. At the same time, plasma perturbations markedly affect atomic spectra susceptible to varying temperature, density, and other factors. Whereas a vast body of literature exists on line broadening in laboratory and astrophysical plasma environments [1–6], there is relatively little work on systematic theoretical treatment of autoionizing resonances that are more readily susceptible to plasma interactions

[7, 8], though results have been obtained for K-shell spectra (viz. [9]) observed astrophysically [10]. Stark broadening and other broadening mechanisms for plasmas have been reviewed from the perspective of individual lines and spectra [11, 12], and in non-local thermodynamic equilibrium [13]. However, opacity calculations require a statistical treatment such as is implemented in the Opacity Project (hereafter OP [6, 14–16]).

Resonances are ubiquitous in cross sections, measured and calculated in a variety of ways with ever-increasing precision and resolution. State-of-the-art experimental devices such as synchrotron based ion storage rings and narrowband photon sources can now resolve resonances in many atomic systems. Coupled-channel (CC) calculations, mainly using the R-Matrix method, have been carried out for nearly all elements and ions up to at least iron under the OP [6, 17] and, more extensively, the Iron Project (hereafter IP [18]). A prime



Original Content from this work may be used under the terms of the [Creative Commons Attribution 4.0 licence](https://creativecommons.org/licenses/by/4.0/). Any further distribution of this work must maintain attribution to the author(s) and the title of the work, journal citation and DOI.

feature of these calculations is the presence of resonances throughout all the energy ranges of interest. However, resonances are of different types, and exhibit varying shapes, sizes and heights. Their overall resonance strengths may also be computed in analogy with line oscillator strengths for modeling of radiative processes [19].

However, the question remains: how are resonance profiles affected by plasma perturbations? To be more precise, how would the *intrinsic* autoionization shape be modified by *extrinsic* particle interactions in a given environment? The complexity of the problem becomes evident when one considers that autoionization profiles are inherently asymmetric, described by the Fano formula for isolated resonances in terms of an asymmetry parameter and energy [20]. However, any singular expression is insufficient to treat an infinite overlapping series of autoionizing (AI) resonances which, in fact, range from extremely narrow Rydberg resonances approaching series limits, to large photoexcitation-of-core resonances that span hundreds of eV in energy and considerably alter the background continuum below the core excitation threshold [19, 21]. Previous work and the conventional approach to plasma modeling of resonances and collisional-radiative models generally follow the ‘isolated resonance approximation,’ which treats autoionizing resonances as discrete bound levels and entail the calculation of the oscillator strength at a single energy, followed by a perturbative plasma broadening treatment based on independently calculated autoionization and radiative rates (viz. the Cowan code [22]). Although a physical explanation is lacking, arbitrarily increasing line broadening factors of all lines by a factor of up to ~ 100 in atomic structure calculations is found to recover the missing solar opacity quantitatively [23].

Ideally, what is needed is a theoretical method that can be translated into a computational algorithm taking into account the variety of resonance shapes and their positions relative to the excited ion core level. Electron–ion interactions in a plasma lead to dominant forms of broadening: Doppler, Stark and electron impact. The Doppler width is approximated by a Gaussian that is more narrowly peaked around the line center and falls off faster than the other Lorentzian profiles due to Stark and electron impact. The Stark effect due to ions is particularly important for hydrogenic systems when it is linear due to l -degeneracy; a static approximation is sometimes employed since ions move much slower than electrons [1, 24]. In contrast, the electron impact broadening profile is Lorentzian with a much wider effect on the line wings, and as the electron density and the temperature of the plasma increase, electron collisions become the dominant source of broadening. This would be especially the case for weakly bound electrons in doubly-excited autoionizing states, which would be more perturbed than the bound electrons considered in line broadening theories.

In this paper we present a computational methodology that aims to incorporate electron impact broadening in a generally applicable manner suitable for laboratory and astrophysical plasma sources. Without a loss of generality and based on large-scale CC R-matrix calculations [21, 25], we consider the photoionization of a complex atomic system from neon-like

to fluorine-like iron, Fe xvii \rightarrow Fe xviii, in this study as an exemplar of its applicability to atomic processes in plasmas.

2. Theoretical formulation

We first sketch out a theoretical outline for the channel coupling that gives rise to resonances, and then the resonance broadening is modeled after line broadening due to electron impact.

2.1. Resonances and channel coupling

Autoionizing resonances manifest themselves via inter-channel coupling in the CC framework. In the CC approximation, the atomic system is represented as the ‘target’ or the ‘core’ ion of N -electrons interacting with the $(N + 1)$ th electron. The $(N + 1)$ th electron may be bound in the electron–ion system, or in the electron–ion continuum depending on its energy being negative or positive. The total wavefunction, Ψ_E , of the $(N + 1)$ -electron system in a symmetry $J\pi$ is an expansion over the eigenfunctions of the target ion, χ_i in specific state $S_iL_i(J_i)\pi_i$, coupled with the $(N + 1)$ th electron function, θ_i :

$$\Psi_E(e + \text{ion}) = A \sum_i \chi_i(\text{ion}) \theta_i + \sum_j c_j \Phi_j, \quad (1)$$

where the \sum_i is over the ground and excited states of the target or the core ion. The $(N + 1)$ th electron with energy k_i^2 corresponds to a channel labeled $S_iL_i(J_i)\pi_i k_i^2 \ell_i(SL(J)\pi)$. The Φ_j s are bound channel functions of the $(N + 1)$ -electron system that account for short range correlation not considered in the first term and the orthogonality between the continuum and the bound electron orbitals of the target.

Depending upon the total energy E of the $(e + \text{ion})$ system, and the channel energy $k_i^2 > 0$ or $k_i^2 < 0$, a channel may be open or closed relative to an ion level E_i . Inter-channel interactions between open and closed channel wavefunctions result in resonances below the excitation threshold at E_i . If $E < 0$ for all channels, then the $(e + \text{ion})$ system is in a pure bound state; otherwise we have a free state with an electron in the continuum and some channels open and some closed. Therefore, the CC wavefunction expansion equation (1) may be used to obtain either $(e + \text{ion})$ collision strengths or bound–bound and bound–free radiative parameters such as oscillator strengths and photoionization cross sections.

With reference to figure 1, we have the position of a given resonance ω_r corresponding to an excitation threshold E_i in terms of its effective quantum number ν_i as

$$\omega_r = \omega_g + E_i - \frac{(z + 1)^2}{\nu_i^2}. \quad (2)$$

That yields

$$\nu_i(\omega_r) = \left[\frac{(z + 1)^2}{\omega_g + E_i - \omega_r} \right]^{1/2}. \quad (3)$$

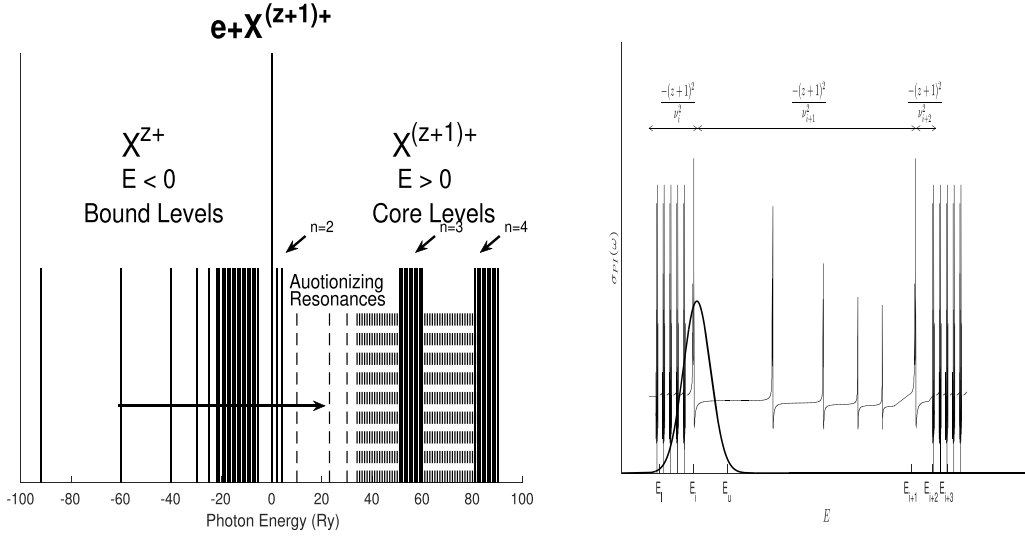


Figure 1. Left: Schematic diagram of a coupled channel calculation for photoionization of bound states (solid lines) of an ion $X^{z+} \rightarrow X^{z+1} + e$ — AI resonances (dashed lines) correspond to Rydberg series converging on to excited levels of the residual ion with $E = -(z+1)^2/\nu^2$. Right: ion thresholds of convergence $E_i, E_{i+1}, E_{i+2}, E_{i+3} \dots$ and a Lorentzian profile with lower and upper energy limits (E_l, E_u) spanning narrow high- n resonances below E_i and broader ones above.

Typically, there are many excited levels E_i included in CC calculations which may number in the hundreds. Infinite series of resonances $E_i \nu_{nl}$ arise and converge on to each level E_i . There can be considerable overlap between weakly bound narrow high- ν Rydberg resonances converging on, to and immediately below a given threshold, and deeply bound strong and wide resonances with low ν -values belonging to higher levels. A computational algorithm must successively convolve groups of resonances identified with respect to all ion core levels.

Let $\tilde{\sigma}(\omega')$ be the computed cross section and $\sigma(\omega)$ the convolved cross section such that

$$\sigma(\omega) = \int \tilde{\sigma}(\omega') \phi(\omega, \omega') d\omega', \quad (4)$$

where the profile factor is

$$\phi(\omega, \omega') = \frac{\gamma(\omega)/\pi}{(\omega - \omega')^2 + \gamma(\omega)^2}. \quad (5)$$

2.2. Resonance broadening mechanisms

A general theoretical approximation for the scattering of a free electron with an electron in doubly-excited quasi-bound states is necessarily computationally intensive since it needs to be incorporated within a CC framework and superimposed on *ab initio* calculations of cross sections. Primary broadening mechanisms such as electron collisions, Stark broadening due to ion microfields, and Doppler broadening due to thermal motions need to be considered *a priori*. We develop a theoretical treatment that accounts for these physical effects independently within a computational viable procedure.

The parameters in the formulation are derived in analogy with line broadening but modified significantly to apply

to AI resonances. In the present formulation, we associate the energy to the effective quantum number relative to each threshold $\omega' \rightarrow \nu_i$ to write the total width as:

$$\gamma_i(\omega, \nu, T, N_e) = \gamma_c(i, \nu, \nu_c) + \gamma_s(\nu_i, \nu_i^*) + \gamma_d(A, \omega) + \gamma_f(f-f; \nu_i, \nu_i'), \quad (6)$$

pertaining to collisional γ_c , Stark γ_s , Doppler γ_d , and free-free transition γ_f widths, with additional parameters as defined below. Without a loss of generality we assume a Lorentzian profile factor that describes collisional-ion broadening which dominates in HED plasmas. We assume this approximation to be valid since collisional profile wings extend much wider as x^{-2} , compared to the shorter range $\exp(-x^2)$ for thermal Doppler, and $x^{-5/2}$ for Stark broadening (viz. [14]). In principle, the limits of integration in equations (4)–(6) are $\mp\infty$, which are replaced in practical calculations by $\mp\gamma_i/\sqrt{\delta}$, where δ is chosen to ensure the full Lorentzian profile energy range and for accurate normalization. Convolution by evaluation of equations (3)–(6) is carried out for each energy ω throughout the tabulated mesh of energies used to delineate all AI resonance structures, for each cross section, and for each core ion threshold.

2.2.1. Electron impact broadening At sufficiently high densities collisional broadening is dominant and mathematically represented by a Lorentzian function (equation (5)) that correctly approximates the slowly varying behavior in the line wings. We develop a numerical procedure for convolving cross sections including resonances over a Lorentzian damping width. Given energy dependent cross sections tabulated at a sufficiently fine mesh, we first switch the energy variable to the effective quantum number $\nu = z/\sqrt{E}$, where $E = \hbar\omega$. In

photoionization, we take ω to be the photon frequency; henceforth we shall also employ ω as the energy variable assuming atomic units $\hbar = 1$. The ν is more appropriate since for a resonance it is defined relative to the excited core ion level, as illustrated in figure 1.

We consider the photoionization of an ion of element X with charge z in an initial state by a photon of energy $\hbar\omega$ into the ground or excited level of a residual ion of charge $(z + 1)$

$$\hbar\omega + X^{z+} \longrightarrow e + X^{z+1}. \quad (7)$$

It is assumed that unperturbed photoionization cross sections $\tilde{\sigma}_{PI}(\hbar\omega)$ are theoretically computed with sufficient resolution in energy to delineate autoionization profiles. According to the impact approximation [6] we may then represent the damping profile with a Lorentzian expression

$$\phi_\omega(E) = \frac{\gamma/\pi}{[(E+x-E_o)^2 + (\gamma^2)]}. \quad (8)$$

By analogy with electron impact damping of bound-bound line transitions, we define E_o as the resonance center, γ as the width and x the energy shift (later we shall assume that $|E - E_o| \gg x$). We may further express

$$N_e\gamma = \gamma + ix, \quad (9)$$

where N_e is the electron density and γ is the damping constant which may be written in terms of the electron distribution $f(\epsilon, T)$ at a given temperature T as

$$\gamma(T) = \int_0^\infty v Q_D(\epsilon) f(\epsilon, T) d\epsilon. \quad (10)$$

Given Q_D as the electron impact cross section and a Maxwellian distribution, we may obtain the thermally averaged damping rate coefficient

$$\Upsilon_D(T) = \int_0^\infty \Omega_D(\epsilon) \exp(-\epsilon/kT) d(\epsilon/kT), \quad (11)$$

where $\Omega(\epsilon)$ is the collision strength. Then

$$\gamma(T) = 2 \frac{\hbar^2}{m} \left(\frac{\pi}{mkT} \right)^{1/2} \Upsilon_D. \quad (12)$$

In equations (8)–(12) the Υ_D is a complex quantity. However, for small $\delta\omega = (\omega - \omega_o)$ in the one-perturber approximation ([6] and references therein), we have $\gamma = N_e\gamma$ and $\phi_\omega = (\gamma/2\pi)/(\omega - \omega_o)^2$.

Now we establish a correspondence between $\gamma(\omega)$ and the electron impact rate coefficient Υ according to the relation

$$\gamma(\omega) = 2 \left(\frac{\pi}{kT} \right)^{1/2} a_o^3 N_e \Upsilon(\nu), \quad (13)$$

where $\Upsilon(\nu)$ is computed at the resonance energy corresponding to $\nu = z/\sqrt{E}$, with E in Rydberg and atomic units $a_o = \hbar = 1$. We now approximate

$$\Upsilon(\nu) \approx G(z) \langle r_\nu^2 \rangle = G(z) \frac{5\nu^4}{2(z+1)^2}. \quad (14)$$

Table 1. Gaunt factor for electron impact collisional broadening: dependence on temperature $T(K)$, ion charge z and effective quantum number ν of excited levels (equation (16)) $T = 2 \times 10^6$ K, $z = 16$.

ν	$G(T, z, \nu)$
3.0	1.75
4.0	2.52
5.0	3.12
6.0	3.60
7.0	4.02
8.0	4.37
9.0	4.69
10.0	4.97

$G(z)$ is an effective Gaunt factor for electron impact excitation of positive ions, empirically determined for line broadening work in the OP [6] to be

$$G(z) = 6.3 - \frac{5.9}{(z+1)}. \quad (15)$$

The behavior of $G(z)$ with ion charge z and temperature T has been further studied for electron impact broadening, and we adopt an improved expression [8, 14, 26]

$$G(T, z, \nu_i) = \sqrt{3}/\pi [1/2 + \ln(\nu_i kT/z)]. \quad (16)$$

For example, in table 1 we compare the two expressions and find that they differ significantly for $\nu < 10$, but $G(T, z, \nu) \rightarrow G(z)$ as $\nu \rightarrow 10$, and exceed marginally for $\nu > 10$ when Breit–Pauli R-matrix (BPRM) resonance structure calculations are truncated.

Here, ω_g is the ionization energy of the ground state of the photoionizing ion X^{z+} . Then, from equation (18) we obtain the temperature-density dependent width at each energy

$$\gamma_i(\omega_r; N_e, T) = 5 \left(\frac{\pi}{kT} \right)^{1/2} a_o^3 N_e G(z) \frac{\nu_i^4(\omega_r)}{(z+1)^2}. \quad (17)$$

Evaluating the constants with $T(K)$ and N_e cm⁽⁻³⁾, we obtain

$$\gamma_i(\omega_r; N_e, T) = 5.2184 \times 10^{-22} \left(\frac{N_e}{T^{1/2}} \right) \left(\frac{G(z)}{(z+1)^2} \right) \nu_i^4(\omega_r). \quad (18)$$

With the transformation of the unbroadened cross section using equation (18),

$$\tilde{\sigma}(\omega) \longrightarrow \sigma(\omega; T, N_e), \quad (19)$$

we obtain the temperature-density-energy dependent functional representing the photoionization cross section broadened by electron impact. This greatly expands the scope of the calculations since equation (19) implies that the convolution must be carried out at each energy in the tabulated energy mesh (transposed as $E(\omega) \rightarrow \nu$) of unbroadened function $\tilde{\sigma}(\omega)$, with another tabulation for the Lorentzian profile

equation (8), and for each temperature and electron density. In the next section we describe the procedure developed for such numerical calculations.

Given N core ion levels corresponding to resonance structures,

$$\sigma(\omega) = \sum_i^N \left[\int \tilde{\sigma}(\omega') \left[\frac{\gamma_i(\omega)/\pi}{x^2 + \gamma_i(\omega)} \right] d\omega' \right]. \quad (20)$$

With $x \equiv \omega' - \omega$, the summation is over all excited thresholds E_i included in the N -level CC or RM wavefunction expansion, and corresponding to total damping width γ_i due to all broadening processes. The profile $\phi(\omega', \omega)$ is centered at each continuum energy ω , convolved over the variable ω' and relative to each excited core ion threshold i .

We employ the following expressions for computations:

$$\gamma_c(i, \nu) = 5 \left(\frac{\pi}{kT} \right)^{1/2} a_0^3 N_e G(T, z, \nu_i) (\nu_i^4 / z^2), \quad (21)$$

where T , N_e , z , and A are the temperature, electron density, ion charge and atomic weight, respectively, and ν_i is the effective quantum number relative to each core ion threshold i : $\omega \equiv E = E_i - \nu_i^2 / z^2$ is a continuous variable. A factor $(n_x / n_g)^4$ is introduced for γ_c to allow for doubly excited AI levels with excited core levels n_x relative to the ground configuration n_g (e.g. for Fe XVIII $n_x = 3, 4$ relative to the ground configuration $n_g = 2$).

2.2.2. Stark broadening A treatment of the Stark effect for complex systems entails two approaches, one where both electron and ion perturbations are combined (viz. [8, 27]), or separately (viz. [6, 14]) employed herein. Excited Rydberg levels are nearly hydrogenic and ion perturbations are the main broadening effect, though collisional broadening competes significantly with increasing density as well as ν_i^4 (equation (14)). For bound levels in a plasma microfield of strength F , the Stark sub-levels of a level n span a range given by the highest component (n, k_{\max}) with energy (viz. [6, 14])

$$E(n, k_{\max}) = -\frac{z^2}{n^2} + \frac{3}{z} n(n-1)F \quad (22)$$

and the lowest component of sub-level $((n+1), k_{\min})$ with energy

$$E(n+1, k_{\min}) = -\frac{z^2}{(n+1)^2} - \frac{3}{z} n(n+1)F. \quad (23)$$

In deriving occupation probabilities in the Mihalas–Hummer–Däppen equation-of-state (MHD-EOS) [16] used in the OP work [6], a critical field strength F_c is calculated when Stark broadening renders these two components equal, and Stark ionization dissolves level n into the continuum. The total Stark width of a given n -complex is $\approx (3F/z)n^2$. Assuming the dominant ion perturbers to be protons with a density equal to electrons, $N_e = N_p$, and replacing n by the effective quantum number ν_i relative to each excited threshold of an ion

with charge z , we take $F = [(4/3)\pi a_0^3 N_e]^2/3$, as employed in MHD-EOS for Stark broadening in equation (6)

$$\gamma_s(\nu_i, \nu_s^*) = [(4/3)\pi a_0^3 N_e]^2/3 \nu_i^2. \quad (24)$$

In addition, by employing equation (6) a Stark ionization parameter $\nu_s^* = 1.2 \times 10^3 N_e^{-2/15} z^{3/5}$ is introduced such that AI resonances may be considered fully dissolved into the continuum for $\nu_i > \nu_s^*$, analogous to but distinct from the Inglis–Teller series limit [28] or the Stark ionization of *bound* (not AI) energy levels, as considered in the MHD-EOS [16].

All calculations are carried out with and without ν_s^* as shown later in table 2 and illustrated in the figures 3–5 presented herein (red and blue curves, respectively). The results are practically indistinguishable with and without the Stark ionization cutoff and the effect on the redistribution of differential oscillator strength or opacity. However, ν_s^* is a parameter that should prove to be useful in further extension of plasma effects, including Debye screening, as discussed later.

2.2.3. Thermal Doppler broadening The Doppler width is:

$$\gamma_d(A, T, \omega) = 4.2858 \times 10^{-7} \sqrt{T/A}, \quad (25)$$

where ω is *not* the usual line center but taken to be each AI resonance energy.

2.2.4. Free–free transition broadening The last term γ_f in equation (6) accounts for free–free transitions among autoionizing levels with ν_i, ν_i' such that

$$X_i + e(E_i, \nu_i) \longrightarrow X_i' + e'(E_i', \nu_i'). \quad (26)$$

The large number of free–free transition probabilities for $+ve$ energy AI levels $E_i, E_i' > 0$ may be computed using RM or atomic structure codes (viz. [29, 30]). Free–free transitions are not considered in the results in figures 2 and 3 but included in the results discussed in table 1, although they are found to be practically negligible.

3. Computational algorithm

In order to elicit and illustrate important physical features of the formulation, we sketch a few salient features of the mathematical algorithm developed to implement the procedure (numerical details and the computer program will be presented elsewhere).

We have re-defined the Lorentzian profile equation (5) as in equation (8), using damping rate coefficient equations (10)–(13) and Maxwellian electron distribution, dependent on electron density and temperature as in equations (17) and (18). A numerical evaluation scheme based on this formulation requires several practical considerations to be incorporated into the computational algorithm and computer program.

3.1. Profile limits

The limits of integration in equation (4) are determined by the extent of the Lorentzian factor in equation (8). It needs to be ensured that the profile extends into the resonance wings and/or approaches the background continuum without a loss of accuracy. Measuring the energy spread relative to the resonance center $\omega = \omega_r$, we note that, according to equation (13) $\omega = \omega_g + E_i$, with respect to the ionization potential and the target excitation energy E_i above the ground state of the residual ion. Then, the profile maximum is (equation (8))

$$\phi_{\max}(\omega = \omega_r) = \frac{1}{\pi\gamma(\omega)}. \quad (27)$$

We introduce an accuracy parameter δ and choose the profile limits $\pm\omega_o$ such that

$$\phi(\omega = \omega_o) = \delta\phi_{\max} = \frac{\delta}{\pi\gamma(\omega)}. \quad (28)$$

Then,

$$\frac{\delta}{\pi\gamma(\omega)} = \frac{\gamma(\omega)/\pi}{(\omega - \omega_o)^2 + \gamma^2(\omega)} \quad (29)$$

or,

$$(\omega - \omega_o)^2 = \gamma^2(\omega) \left(\frac{1}{\delta} - 1 \right). \quad (30)$$

For small δ ,

$$(\omega - \omega_o)^2 \approx \frac{\gamma^2(\omega)}{\delta}. \quad (31)$$

Therefore, $|\omega - \omega|$ limits the convolution profile such that

$$\omega - \omega_o = \pm \frac{\gamma}{\delta^{1/2}}. \quad (32)$$

Whereas equation (4) using equation (5) has an analytical solution in terms of $\tan^{-1}(x/\gamma)/\gamma$ evaluated at limiting values of $x \rightarrow \mp\gamma/\sqrt{\delta}$, its evaluation for practical applications entails piece-wise integration across multiple energy ranges spanning many excited thresholds and different boundary conditions. For example, the total width γ is very large at high densities and the Lorentzian profile may be incomplete above the ionization threshold and therefore not properly normalized. We obtain the necessary redward left-wing correction for partial renormalization as

$$\lim_{a \rightarrow -\gamma/2\sqrt{\delta}} \int_a^{+\gamma/\sqrt{\delta}} \phi(\omega, \omega') d\omega' = \left[\frac{1}{4} - \frac{\tan^{-1}\left(\frac{a}{\gamma/2\sqrt{\delta}}\right)}{\pi} \right], \quad (33)$$

where a is the lower energy range up to the ionization threshold, reaching the maximum value $-\gamma/2\sqrt{\delta}$. The parameter δ is generally chosen to be 10^{-2} so that the total profile ranges over 10γ .

3.2. Convolution quadrature

The complexity of the problem arises from the following main factors: (i) the wide variety of narrow and broad resonances, (ii) overlapping infinite Rydberg series belonging to a large number of excitation thresholds of the target ion, and (iii) Lorentzian profiles that vary at each energy on a mesh that is independent of the tabulated energy mesh for the original cross section. The schematics are described in figure 2.

Numerically, we need to evaluate the integrand in equation (20) using equation (9), i.e.

$$\sigma(\omega) = \sum_i \left[\int \tilde{\sigma}(\omega') \left[\frac{\gamma_i(\omega)/\pi}{(\omega - \omega')^2 + \gamma_i^2(\omega)} \right] d\omega' \right]. \quad (34)$$

Here, the summation is over all excitation thresholds E_i included in the CC wavefunction expansion (equation (1)) and corresponding damping widths γ_i . The profile $\phi(\omega', \omega)$ is centered at ω ; we define $x \equiv \omega' - \omega$ (note the change of the order of variables which is immaterial), then

$$\sigma(\omega) = \sum_i \left[\frac{\gamma_i}{\pi} \int_{-\frac{\gamma_i}{\sqrt{\delta}}}^{+\frac{\gamma_i}{\sqrt{\delta}}} \frac{\tilde{\sigma}(x)}{x^2 + \gamma_i^2} dx \right]. \quad (35)$$

This equation requires discrete summation over all target ion thresholds, and piecewise integration over the normalized profile at each energy. First, we consider the endpoints with lower energy limit $x_\ell \equiv -(\omega_o - \omega) = -\gamma_i/\sqrt{\delta}$, and upper limit $x_u \equiv +(\omega_o - \omega) = +\gamma_i/\sqrt{\delta}$. Let the tabulated energy mesh be $\omega_1, \omega_2, \dots, \omega_N$. Then $x_1 = \omega_1 - \omega$, $x_2 = \omega_2 - \omega$, ..., $x_N = \omega_N - \omega$. Assuming the lower limit x_ℓ to lie between $x_1 < x_\ell < x_2$; and the upper limit x_u between $x_{N-1} < x_u < x_N$, we have

$$\sigma(\omega) = \sum_i \left[\frac{\gamma_i}{\pi} \int_{x_\ell}^{x_2} \frac{\tilde{\sigma}(x)}{x^2 + \gamma_i^2} dx + \int_{x_3}^{x_4} (\dots) dx + \dots \right] \quad (36)$$

$$+ \dots + \left[\int_{x_{N-1}}^{x_N} (\dots) dx \right]. \quad (37)$$

3.3. Interpolation and evaluation

Each of the raw originally tabulated unbroadened cross sections $\tilde{\sigma}(\omega')$ needs to be interpolated on to the resonance profile mesh. A linear interpolation is sufficient for precision since the CC calculations are usually carried out at a fine mesh to resolve most autoionizing resonances up to $\nu_i \leq \nu_{\max} = 10$ below each target threshold E_i . Suppose the transposed energy mesh ω on to the resonance profile is represented by linearly interpolated segments $a_j + b_j x$ with a_j, b_j coefficients such that, $x_\ell = -\gamma/\sqrt{\delta} < x < x_2 \rightarrow \sigma_1(\omega) = a_1 + b_1 x$, $b_1 = [\tilde{\sigma}(\omega_2) - \tilde{\sigma}(\omega_1)]/(\omega_2 - \omega_1)$; $x_2 < x < x_3 \rightarrow \sigma_2(\omega) = a_2 + b_2 x$, $b_2 = [\tilde{\sigma}(\omega_3) - \tilde{\sigma}(\omega_2)]/(\omega_3 - \omega_2)$; $x_{(N)} < x < x_u = +\gamma/\sqrt{\delta} \rightarrow \sigma_N(\omega) = a_N + b_N x$, $b_N = [\tilde{\sigma}(\omega_N) - \tilde{\sigma}(\omega_{N-1})]/(\omega_N - \omega_{N-1})$. Then, for all thresholds i ,

$$\sigma(\omega) = \sum_i \frac{\gamma_i}{\pi} [\sigma_1(\omega) + \sigma_2(\omega) + \dots + \sigma_N(\omega)]. \quad (38)$$

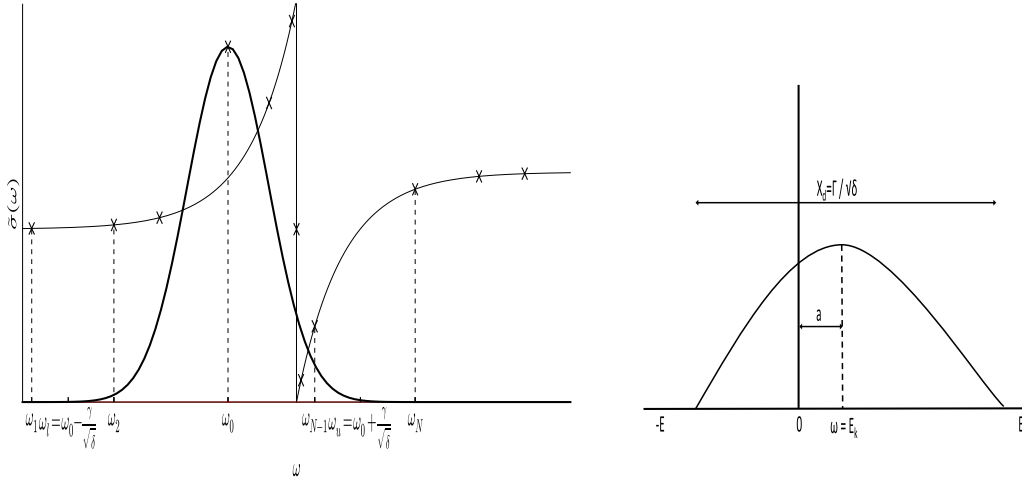


Figure 2. Left: Tabulated cross sections at energies ($\hbar b a = 1$) $\omega_1, \dots, \omega_N$ spanning a resonance centered at ω_o , and Lorentzian profile with lower and upper limits $\omega_l = \omega_o - \gamma/\text{sqrt}(\delta)$, $\omega_u = \omega_o + \gamma/\text{sqrt}(\delta)$. Point-by-point normalized profile convolution ensures a complete quadrature. Right: incomplete profile centered at $\omega = E_k$ with lower energy redward cut-off at ionization threshold on the left and partial renormalization as in equation (31).

It is understood that the interpolation and summation is carried out with respect to profiles corresponding to all target ion thresholds at E_i . Having determined coefficients a_j, b_j we need to evaluate expressions for each segment as

$$\sigma_j(\omega) = \frac{\gamma_i}{\pi} \int_{x_j}^i x^{j+1} \frac{(a_j + b_j x)}{x^2 + \gamma^2} dx. \quad (39)$$

Evaluating separately,

$$\sigma_j(\omega) = a_j \left[\frac{\tan^{-1}(x/\gamma_i)}{\gamma_i} \Big|_{x_j}^{x_{j+1}} \right] + \frac{b_j}{2} \left[\ln(x^2 + \gamma_i^2) \Big|_{x_j}^{x_{j+1}} \right]. \quad (40)$$

For clarity we have avoided the use of double scripts (i, j), one with respect to thresholds E_i and the other for interpolation between respective resonance profile segments. But in principle we may represent the final values of the cross sections convolved over all resonances at the transposed energy mesh $\omega' \rightarrow \omega$ as

$$\sigma(\omega) = \sum_{i,j} \sigma_j^i(\omega), \quad (41)$$

subsuming all target ion levels (figure 1 and equation (1)) and interpolation into the computational algorithm. Finally, we compute broadened cross sections at the same energy mesh as the unbroadened cross sections $\tilde{\sigma}(\omega')$ so that there is one-to-one correspondence $\omega' \rightarrow \omega$. However, we note that the *intermediate* energy mesh of the Lorentzian profile is independent and interpolated in accordance with the damping width equations (11) and (12) at each energy.

3.4. Computer program

A general program for convolving AI resonances has been written and will be reported elsewhere. Here we note a few of the main features. The primary loops in the program are

over electron temperature T_e , density N_e , and target thresholds E_i . The input is the unbroadened CC cross sections tabulated at a sufficiently fine mesh to resolve resonances so that convolution, interpolation and integration do not result in a loss of accuracy. The accuracy parameter δ is chosen to be in the range $10^{-2} - 10^{-6}$; more importantly, it is ensured that the convolved cross sections have converged, physically implying that the resonance wings have merged into the continuum. The CPU time required depends mainly on the density which determines the total width γ ; for example, in the reported calculations for Fe xvii at $T = 2 \times 10^6$ K it is a few minutes for $N_e = 10^{21}$ cc and ~ 3 h for $N_e = 10^{24}$ cc.

The program is suitable as a module within a post-processing program for CC cross sections with AI resonances for photoionization, electron-ion collisions and recombination, intended for practical application in a specified temperature-density range.

4. Results and discussion

The complexity and magnitude of RMOP computations have been studied using photoionization data for a large number of bound levels of the three Fe ions described in RMOP2 [31–35]. Since AI plasma broadening must be carried out at each temperature-density pair, the resulting cross sections constitute a huge amount of data required for opacity calculations in HED plasma sources. In this section we discuss a small sample of results for those Fe ions to illustrate some physical features.

4.1. Fe xvii : temperature-density dependence

Due to its closed shell ground configuration and many excited n -complexes of configurations, Ne-like Fe xvii is of considerable importance in astrophysical and laboratory plasmas, as described in a number of previous works ([36] and references therein). The Fe xvii BPRM calculations

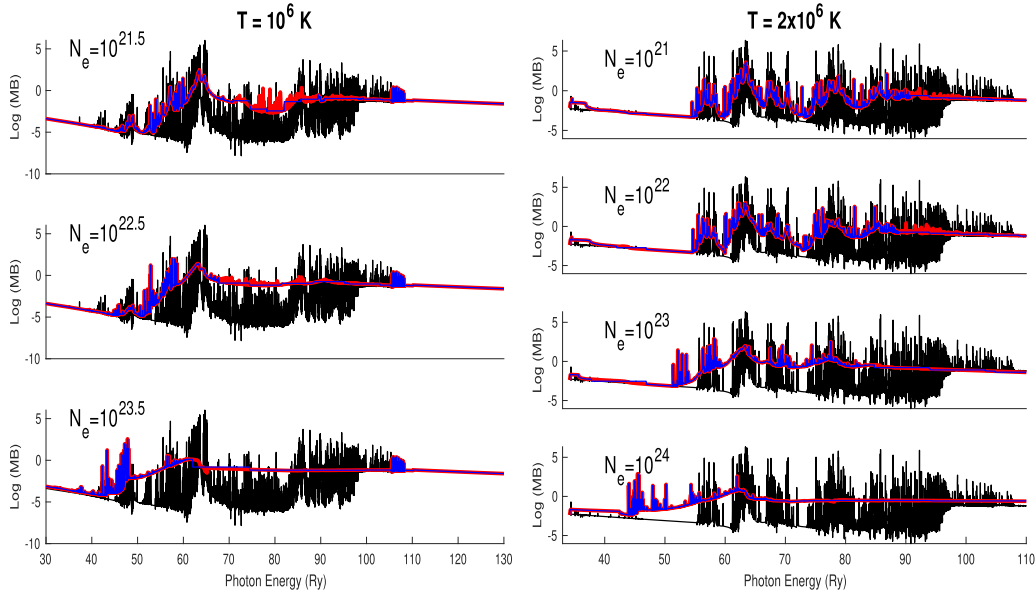


Figure 3. Plasma broadened photoionization cross sections for $\hbar\omega + \text{Fe XVII} \rightarrow e + \text{Fe XVIII}$ of the bound level $2s^22p^5[{}^2P_{3/2}^o]4d({}^1F^o_3)$ (left, ionization energy 17.626 Ry), level $2s^22p^5[{}^2P_{3/2}^o]3p({}^3D_2)$ (right, ionization energy 37.707 Ry) along two isotherms $T = 1 \times 10^6$ K (left) and $T = 2 \times 10^6$ K (right), and electron densities as shown in each panel: black — unbroadened, red—broadened, blue—broadened with Stark ionization cut-off ν_s^* (table 1). Rydberg series of AI resonance complexes with $\nu_i \leq 10$ belonging to 217 excited Fe XVIII levels E_i broaden and shift with increasing density, also resulting in continuum raising and threshold lowering.

are carried out with 218 fine structure levels dominated by $n = 2, 3, 4$ levels of the core ion Fe XVIII. The computed Fe XVII bound levels ($E < 0$) are dominated by configurations $1s^22s^22p^6({}^1S_0)$, $1s^22s^22p^q n\ell, [SLJ]$ ($p, q = 0-2$, $n \leq 10$, $\ell \leq 9$, $J \leq 12$). The core Fe XVII levels included in the CC calculation for the $(e + \text{Fe XVIII}) \rightarrow \text{Fe XVII}$ system are: $1s^22s^22p^5({}^2P_{1/2,3/2}^o)$, $1s^22s^22p^q n\ell, [S_iL_iJ_i]$ ($p = 4, 5$, $n \leq 4$, $\ell \leq 3$). The Rydberg series of AI resonances correspond to $(S_iL_iJ_i) n\ell$, $n \leq 10$, $\ell \leq 9$, with effective quantum number defined as a continuous variable $\nu_i = z/\sqrt{(E_i - E)}$ ($E > 0$), throughout the energy range up to the highest 218th Fe XVIII core level; the $n = 2, 3, 4$ core levels range from $E = 0-90.7$ Ry [21, 36]. The Fe XVII BPRM calculations were carried out resolving the bound-free cross sections at ~ 40000 energies for 454 bound levels with AI resonance structures (in total 587 bound levels are considered, but the higher lying levels are included to ensure convergence and completeness as discussed in paper P4, and do not significantly contribute to opacity calculations). Given 217 excited core levels of Fe XVIII, convolution is carried out at each energy or approximately 10^9 times for each (T, N_e) pair.

Figure 3(left) displays detailed results for plasma broadened and unbroadened photoionization cross section of one particular excited level $2s^22p^5[{}^2P_{3/2}^o]3p({}^3D_2)$ (left, ionization energy 37.707 Ry) of Fe XVII along isotherm $T = 10^6$ K at three representative densities (note the ~ 10 orders of magnitude variation in resonance heights along the Y-axis). The main features evident in the figure are as follows. (i) AI resonances begin to show significant broad-

ening and smearing of a multitude of overlapping Rydberg series at $N_e = 10^{21}$ c.c. The narrower high- n l resonances dissolve into the continua but the stronger low- n l resonances retain their asymmetric shapes with attenuated heights and widths. (ii) As the density increases by one to two orders of magnitude, to $N_e = 10^{22-23}$ cc, resonance structures not only broaden but their strengths shift and are redistributed over a wide range determined by the total width $\gamma(\omega, \nu_i, T, N_e)$ at each energy $\hbar\omega$ (equation (6)). (iii) Stark ionization cutoff (table 1) results in step-wise structures that represent the average due to complete dissolution into continua. (iv) The total AI resonance strengths are conserved, and integrated values generally do not deviate by more than 1%–2%. For example, the three cases in figure 3(left): unbroadened structure (black) and broadened without (red) and with Stark cutoff (blue), the integrated numerical values are 59.11, 59.96, 59.94, respectively. This is also an important accuracy check for numerical integration and the computational algorithm as well as the choice of the parameter δ that determines the energy range of the Lorentzian profile at each T and N_e ; in the present calculations it varies from $\delta = 0.01-0.05$ for $N_e = 10^{21-24}$ cc.

Figure 3(right) shows similar results to figure 3 (left) for another excited Fe XVII level $2s^22p^5[{}^2P_{3/2}^o]4d({}^1F^o_3)$ (ionization energy 17.626 Ry), along a higher temperature 2×10^6 K isotherm at different intermediate densities. Both figures 2 and 3 show a redward shift of low- n resonances and dissolution of high- n resonances. In addition, the background continuum is increased owing to the redistribution of resonance strengths, which merge into one across high lying and overlapping thresholds.

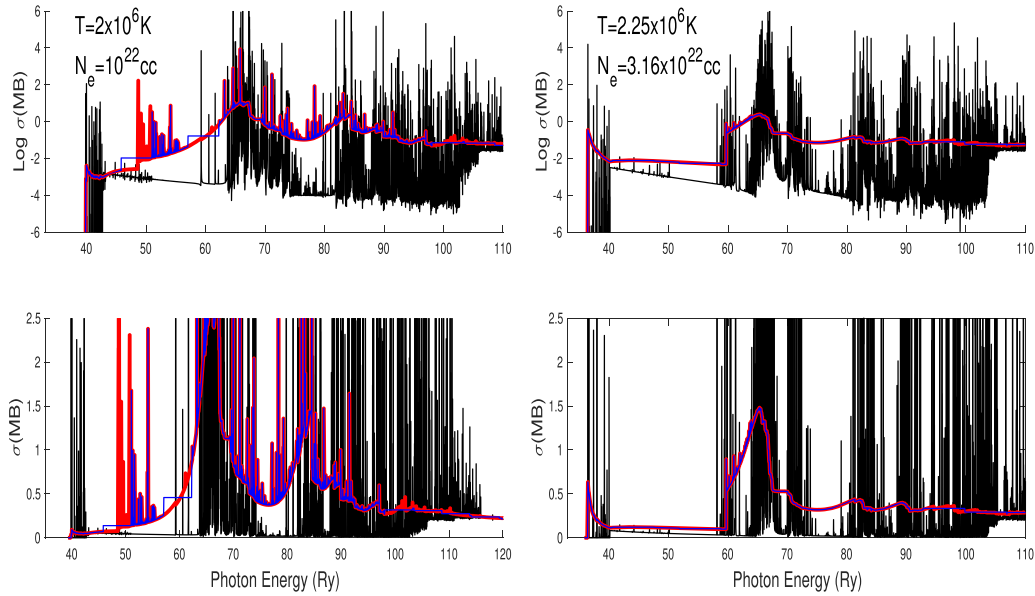


Figure 4. Plasma broadened photoionization cross sections on Log and linear scales, $\sigma_{PI}(\text{MB})$ (top panels) and $\text{Log}\sigma_{PI}(\text{MB})$ (bottom panels) for $\hbar\omega + \text{Fe XVIII} \rightarrow e + \text{Fe XIX}$ of the bound level $2s^2p^5\ ^2P^{\circ}_{1/2}$ (left, ionization energy 98.903 Ry), and level $2s^22p^4(^1D_2)3p^2F^{\circ}_{5/2}$ (right, ionization energy 39.1204 Ry): black — unbroadered, red—broadened, blue—broadened with Stark ionization cut-off ν_i^* (table 1). Rydberg series of AI resonance complexes with $\nu_i \leq 10$ belonging to 276 excited Fe XIX levels.

4.2. Fe XVIII : scaling and delineation of resonances

Next, we employ plasma broadened cross sections for Fe XVIII to highlight the scale, shape, scope, width and magnitude of AI resonances.

The scale of unbroadered AI features is evident upon a comparison on log and linear scales as in figure 4 (black curves), considered for two excited Fe XVIII levels. The top and bottom panels on left and right exhibit $\text{Log}\sigma_{PI}(\text{MB})$ and $\sigma_{PI}(\text{MB})$, respectively. Whereas the log-scale of the top panels appropriately displays the full extent of AI resonances, it appears with equal weight for both positive values that rise up to 10^6 MB, and for negative values down to 10^{-6} MB that are not significant contributors, as shown in the bottom panels on a much smaller linear scale going from zero only up to 2.5 MB.

Attenuation of AI features due to plasma effects is shown in the red and blue curves at two different $T - D$ pairs; cross sections on the left are at a lower temperature and more than three times lower electron density than the ones on the right. Consequently, the AI features on the right in figure 4 are much more broadened than the ones on the left. Two other noticeable features are the closing of ‘opacity windows’ in the unbroadered cross sections, and the shift of AI resonances leading to temperature-density dependent redistribution of differential oscillator strengths and opacity with energy.

4.3. Conservation of differential oscillator strength

It is important to ensure the numerical accuracy of AI plasma broadening in temperature-density-energy space. Theoretically and computationally, that implies an investigation of integrated differential oscillator strengths proportional

to σ_{PI} for all levels of a given ion for the three forms computed: (i) unbroadered (black curves), (ii) with all plasma broadening effects included as in equation (6) (red curves), and (iii) as in (ii) but with Stark ionization cutoff that leads to sharp step-wise structures below each ionization threshold (blue curves). We have quoted these values for one level of Fe XVII above in figure 3.

In figure 5 we present σ_{PI} for the ground state of Fe XIX $2s^2p^4\ ^3P^3$ (ionization energy 104.956 Ry), as well as an excited state $2s2p^4(^2S)3s\ ^1S^e$ (ionization energy 24.186 Ry). For these two cross sections of Fe XIX we find integrated values over the entire energy range shown to be 21.74, 22.98 and 22.90 for the unbroadered, broadened, and broadened with Stark ionization cutoff, for the ground state, and 12.48, 13.57 and 13.56, respectively, for the excited state (units are in MB-Ry though only the relative values are indicators of accuracy). The numerical agreement between the three sets of values is well within $\sim 10\%$ indicating the conservation of oscillator strength, despite some uncertainty in integration over extensive narrow and broad resonance structures that vary by nearly 20 orders of magnitude in height for $\sigma_{PI}(2s2p^4(^2S)3s\ ^1S^e)$, and widely disparate width distribution among Rydberg vs. Seaton PEC resonances described in RMOP2.

Generally, the agreement between the three sets of calculations for each level of each ion at each temperature-density is also an accuracy check of the plasma broadening treatment presented. Since there are hundreds of levels for each ion considered, there is more than 10% difference in integrated cross sections for highly excited levels at very high densities where the total AI width (equation (6)) is very large. However, the highly excited levels are cut-off by the MHD-EOS and not considered in opacity calculations.

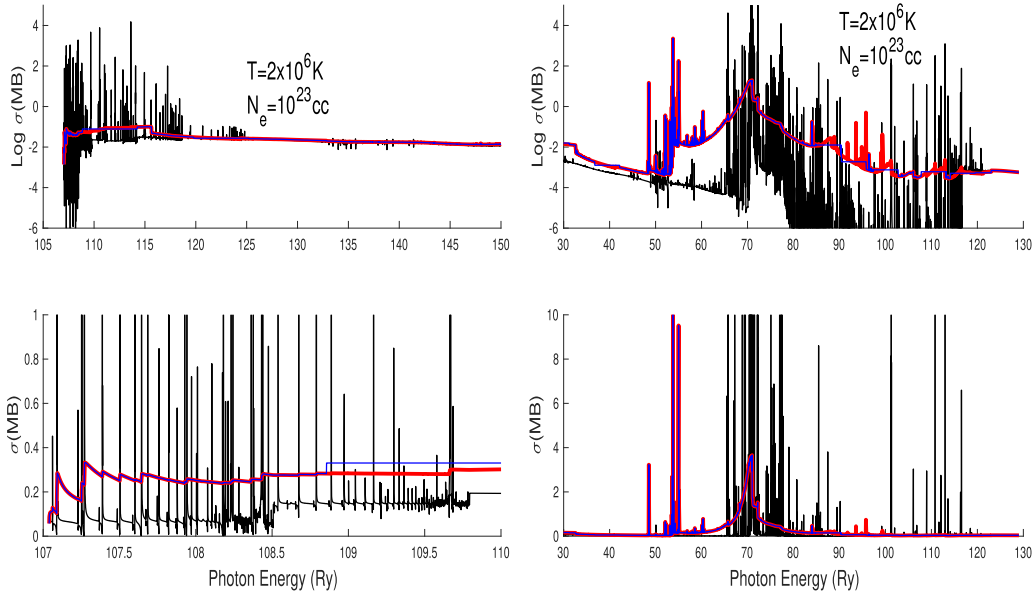


Figure 5. Plasma broadened photoionization cross sections on Log and linear scales, $\sigma_{PI}(\text{MB})$ (top panels) and $\text{Log}\sigma_{PI}(\text{MB})$ (bottom panels) for $\hbar\omega + \text{Fe XIX} \rightarrow e + \text{Fe XX}$ of the ground state $2s^2p^4\ ^3P^e$ (left), and $2s2p^4(^2S)3s\ ^1S^e$ (right): black — unbroadened, red—broadened, blue—broadened with Stark ionization cut-off ν_s^* (table 1). All resonances in the unbroadened σ_{PI} on the right range over 20 orders of magnitude.

4.4. Plasma opacity parameters

Table 2 gives plasma parameters corresponding to figure 3. Their physical significance is demonstrated by a representative sample tabulated at temperatures $T(K)$ and N_e . The maximum width γ_{10} corresponding to $\nu_i = 10$ in equations (3) and (6) is set by the CC-BPRM calculations which delineate unbroadened AI resonance profiles up to $\nu \leq 10$, and employ an averaging procedure up to each threshold $10 < \nu < \infty$ using quantum defect theory (viz. [6, 19, 37] and references therein). $\gamma_c(10)$ and $\gamma_s(10)$ are the maximum collisional and Stark width components. The Doppler width γ_d is much smaller, 1.18×10^{-3} and 1.67×10^{-3} Ry at 10^6 K and 2×10^6 K, respectively, validating its inclusion in equation (6) in HED plasma sources but possibly not when γ_d is comparable to γ_c or γ_s . The ν_s^* and ν_D are effective quantum numbers corresponding to the Stark ionization cutoff and the Debye radius, respectively. We obtain $\nu_D = [\frac{2}{5}\pi z^2 \lambda_D^2]^{1/4}$, where the Debye length $\lambda_D = (kT/8\pi N_e)^{1/2}$. It is seen in table 2 that $\nu_D > \nu_s^*$ at the T, N_e considered, justifying the neglect of plasma screening effects herein, but which may need to be accounted for at even higher densities.

The aggregate effect of AI broadening for large-scale applications is demonstrated in table 2 by the ratio R of the Rosseland Mean Opacity (defined and discussed in RMOP1 equations (1)–(4)), at different temperatures and densities, using broadened/unbroadened cross sections for 454 Fe XVII levels with AI resonances (other higher bound levels have negligible resonances) [36, 38]. For any atom or ion, R is highly dependent on T and N_e ; for Fe XVII R yields up to 58% enhancement due to plasma broadening with increasing N_e along the 2×10^6 K isotherm, but decreasing to 6% along

Table 2. Plasma parameters along isotherms in figures 2 and 3; ν_D corresponds to Debye radius; R is the ratio of Fe XVII Rosseland Mean Opacity with and without broadening [38]; γ_{10} is the maximum AI resonance width at $\nu = 10$.

$T(K)$	$N_e(\text{cc})$	$\gamma_{10}(\text{Ry})$		$\gamma_s(10)$	ν_s^*	ν_D	R
		$\nu = 10$	$\gamma_c(10)$				
2×10^6	10^{21}	3.42(-1)	8.55(-2)	2.57(-1)	10.4	28.1	1.35
2×10^6	10^{22}	2.05(0)	8.55(-1)	1.19(0)	7.7	15.8	1.43
2×10^6	10^{23}	1.41(1)	8.55(0)	5.53(0)	5.6	8.9	1.55
2×10^6	10^{24}	1.11(2)	8.55(1)	2.57(1)	4.1	5.0	1.58
10^6	$3.1 \times 10^{21.5}$	8.17(-1)	2.71(-1)	5.46(-1)	9.0	17.8	1.47
10^6	$3.1 \times 10^{22.5}$	5.25(0)	2.71(0)	2.53(0)	6.6	10.0	1.13
10^6	$3.1 \times 10^{23.5}$	3.89(0)	2.71(1)	1.18(0)	4.8	5.6	1.06

the 10^6 K isotherm. Approximately 70 000 free-free transitions among +ve energy levels are included in the calculation of R , but their contribution has no significant broadening effect since they entail very high-lying levels with negligible level populations. However, different plasma environments with intense radiation fields, or a different equation-of-state than [16] employed here, may lead to more discernible effects due to free-free transitions. AI broadening in a plasma environment affects each level cross section differently, and hence its contribution to opacity and rate equations for atomic processes in general. A critical (T, N_e) range can therefore be numerically ascertained where redistribution and shifts of atomic resonance strengths would be significant and cross sections should be modified. The overall opacity enhancement depends not only on AI resonance broadening at a given temperature-density but also on the equation-of-state [39].

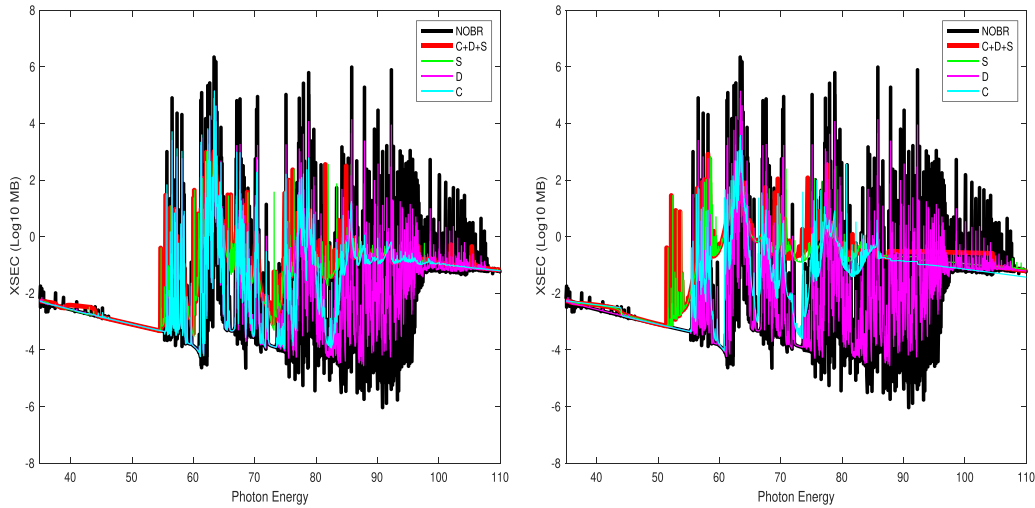


Figure 6. Effect of including individual broadening mechanisms on photoionization cross sections in figure 3 for isotherm $T = 2 \times 10^6$ K, $N_e = 10^{22}/\text{cc}$ (Left) and $N_e = 10^{23}/\text{cc}$ (Right): unbroadened (black), total broadened (red), C—Collisional (cyan), D—Doppler Thermal (magenta), S—Stark (green).

4.5. Relative broadening effects

Following table 1 we can examine the individual effects of including different broadening mechanisms separately in the combined total (equation (6)). Figure 6 shows the cross sections including the three dominant mechanisms. Referring to figure 3 for photoionization of Fe XVIII and table 1, the contributions are shown to be due to equation (21) for collisional (cyan), equation (25) for thermal (magenta), and equation (24) for Stark (green) effects, respectively. Results are given in figure 6 for $T = 2 \times 10^6$ K at two electron densities $10^{21}/\text{cc}$ (left) and $10^{23}/\text{cc}$ (right). From table 1 we see the relative widths due to collisional and Stark broadening; thermal (Doppler) broadening is much smaller and manifests itself only for very narrow resonances and high-lying thresholds. At lower density (left) many of the unbroadened resonance structures (black) are discernible although significantly dissolved, and the collisional width is less than the Stark width, which is larger (table 1) and closer to the total broadened cross sections (red). At higher density (right) the effects of collisional and Stark are reversed; the former is more prominent though quite comparable to the latter. More detailed studies on a number of cross sections for different ions would be needed to ascertain precisely the broadening effects in each case. However, from the limited results presented herein a conservative estimate is that the lower density limit for broadening mechanisms to manifest themselves is $N_e > 10^{20}/\text{cc}$. Table 1 also indicates probable high density limit at $N_e > 10^{24}/\text{cc}$ based on two reasons: (i) the total combined AI broadening widths become very large and comparable to the entire energy range of the resonance structures included in the computations of cross sections, and (ii) the Debye lengths are comparable to or shorter than bound electronic orbital radii, and atomic configurations are no longer a viable description which would require dense plasma effects to be considered non-perturbatively.

5. Conclusion

The main conclusions are: (I) The method described herein is generally applicable to AI resonances in atomic processes in HED plasmas. (II) The cross sections become energy-temperature-density dependent in a critical range leading to broadening, shifting, and dissolving into continua. (III) Among the approximations necessary to generalize the formalism is the assumption that thermal Doppler widths are small compared to collisional and Stark widths as herein, but given the intrinsic asymmetries of AI resonances it may not lead to significant inaccuracies (although this needs to be verified in future works). (IV) The treatment of Stark broadening and ionization cutoff is ad hoc, albeit based on the equation-of-state formulation [16] and consistent with previous works [6]. (V) Since it is negligibly small, the free-free contribution is included post-facto in the computation of the ratio R in table 2 and not in the cross sections and results shown in figures 2 and 3, but may be important in special HED environments with intense radiation and should then be incorporated in the main calculations of total AI width (equation (6)). (VI) The predicted redward shift of AI resonances as the plasma density increases should be experimentally verifiable. (VII) The redistribution of AI resonance strengths should particularly manifest itself in rate coefficients for ($e + \text{ion}$) excitation and recombination in plasma models and simulations and for photoabsorption in opacity calculations, using temperature-dependent Maxwellian, Planck, or other particle distribution functions. (VIII) The treatment of individual contributions to AI broadening may be improved, and the theoretical formulation outlined here is predicated on the assumption that external plasma effects are perturbations subsumed by and overlying the intrinsic autoionization effect. (IX) The computational formalism is designed to be amenable to practical applications and the computational algorithm and general-purpose program

AUTOBRO are optimized for large-scale computations of AI broadened cross sections for atomic processes in HED plasma and astrophysical models.

Data availability statement

All data that support the findings of this study are included within the article (and any supplementary files).

Acknowledgments

I would like to thank Sultana Nahar for atomic data for Fe ions and discussions.

ORCID iD

A K Pradhan  <https://orcid.org/0000-0001-8775-3643>

References

- [1] Griem H R 2005 *Principles of Plasma Spectroscopy* (Cambridge University Press)
- [2] Peach G 1981 *Adv. Phys.* **30** 367
- [3] Konjevic N 1999 *Phys. Rep.* **316** 339
- [4] Djurovic S and Konjevic N 2009 *Plasma Sources Sci. Technol.* **18** 030511
- [5] Drake R P 2006 *High Energy Density Physics* (Springer)
- [6] The Opacity Project Team 1995 *The Opacity Project* vol 1 (Institute of Physics Publishing)
- [7] Kelleher D E, Depeche J F and Weiner J 1985 *Phys. Rev. A* **32** 2230
- [8] Xiang W, Zeng J, Fu Y and Gao C 2012 *J. Mod. Phys.* **3** 1670
- [9] Palmeri P, Quinet P, Mendoza C, Bautista M, Withoef M C and Kallman T R 2016 *Astron. Astrophys.* **589** A137
- [10] Gatuzz E, Gorczyca T W, Hasoglu M F, Schulz N S, Corrales L and Mendoza C 2020 *Mon. Not. R. Astron. Soc.* **498** L20
- [11] Gigosos M A 2014 *J. Phys. D* **47** 343001
- [12] Cooper J W and Saloman E B 1982 *Phys. Rev. A* **26** 1452
- [13] Ivan H and Dimitri M 2015 *Theory of Stellar Atmospheres* (Princeton University Press)
- [14] Seaton M J 1990 *J. Phys. B* **23** 3255
- [15] The OP work [6] consists of treatment of line broadening implemented by M J Seaton in four papers in the series *Atomic Data for Opacity Calculations* (ADOC) — ADOC-I, ADOC-V, ADOC-VIII and ADOC XIII [14]
- [16] Mihalas D, Hummer D G and Däppen W 1988 *Astrophys. J.* **331** 815
- [17] Seaton M J, Yu Y, Mihalas D and Pradhan A K (SYMP) 1994 *Mon. Not. R. Astron. Soc.* **266** 805
- [18] Hummer D G, Berrington K A, Eissner W, Pradhan A K, Saraph H E and Tully J A 1993 *Astron. Astrophys.* **279** 298
- [19] Pradhan A K and Nahar S N 2011 *Atomic Astrophysics and Spectroscopy* (Cambridge University Press)
- [20] Fano U 1961 *Phys. Rev. A* **124** 1866
- [21] Nahar S N, Pradhan A K, Chen G-X and Eissner W 2011 *Phys. Rev. A* **83** 053417
- [22] Cowan R D 1981 *The Theory of Atomic Structure and Spectra* (University of California Press)
- [23] Krief M, Feigel A and Gazit D 2016 *Astrophys. J.* **824** 98
- [24] Hubney I and Mihalas D 2014 *Theory of Stellar Atmospheres* (Princeton University Press) Mihalas D 1978 *Stellar Atmospheres* (Freeman)
- [25] Burke P G 2011 *R-Matrix Theory of Atomic Collisions* (Springer)
- [26] Dimitrijevic M S and Konjevic N 1981 *Astron. Astrophys.* **102** 93
- [27] Dimitrijevic M S and Konjevic N 1987 *Astron. Astrophys.* **172** 345
- [28] Inglis D R and Teller E 1939 *Astrophys. J.* **90** 439
- [29] Seaton M J 2000 *J. Phys. B* **33** 2677
- [30] Eissner W, Jones M and Nussbaumer H 1974 *Comput. Phys. Commun.* **8** 270
- [31] Several formulations were investigated and employed to implement a Voigt profile used in line broadening work (viz. [36–38] and later works). They were found to be numerically unstable owing to required limits on the relative widths of AI broadening mechanisms considered herein, that rendered the Voigt kernel mathematically ill-conditioned and computationally impractical. For example, the parameter related to the ratio collisional-to-Doppler widths γ_c/γ_d , that is usually evaluated and specified for line broadening and assigned numerical limiting values in integration, is not practical since $\gamma_c \gg \gamma_d$ at temperatures and densities of interest in HED plasmas
- [32] Hummer D 1965 *Mon. Not. R. Astron. Soc.* **70** 1
- [33] Hui A K, Armstrong B H and Wray A A 1978 *J. Quantum Spectrosc. Radiat. Transfer* **19** 509
- [34] Huang X and Yung Y L 2004 *Am. Meteorol. Soc.* **61** 1630
- [35] Yu Y and Seaton M J 1987 *J. Phys. B* **20** 6409
- [36] Nahar S N and Pradhan A K 2016 *Phys. Rev. Lett.* **116** 235003 Nahar S N and Pradhan A K 2016 *Phys. Rev. Lett.* **117** 249502
- [37] The QD regions $10 < \nu_i < \infty$ are generally small and overlapping for closely spaced excited core levels, as herein
- [38] We eschew a discussion of opacities *per se*, as they also depend on accuracy and completeness of atomic data, equation-of-state of the plasma source and other quantities, and focus on AI resonance broadening in atomic processes
- [39] Pradhan A K 2024 *Mon. Not. R. Astron. Soc.* **527** L179